

Kinetic Study of the Oxidation of Water by Ce^{IV} Ions Mediated by Activated Ruthenium Dioxide Hydrate

Andrew Mills* and Neil McMurray

Department of Chemistry, University College of Swansea, Singleton Park, Swansea, SA2 8PP

The results of a kinetic study of the oxidation of water to oxygen by Ce^{IV} ions, mediated by thermally activated ruthenium dioxide hydrate (RuO₂·*γ*H₂O*), are reported. At low [Ce⁴⁺], *i.e.* ca. 3.45 × 10⁻⁵ mol dm⁻³, the rate of reduction of Ce^{IV} ions (*R*) was diffusion controlled and depended directly upon [Ce⁴⁺] and [redox catalyst], but was virtually independent of [Ce³⁺]. At higher [Ce⁴⁺], *i.e.* 3.45 × 10⁻³ mol dm⁻³, the kinetics were more complex, with *R* decreasing with increasing [Ce³⁺] and decreasing [Ce⁴⁺] and [redox catalyst]. The observed kinetics can be successfully described using an electrochemical model in which the catalyst particles are considered to act as microelectrodes which mediate the transfer of electrons between a Nernstian reaction (the reduction of Ce^{IV} ions) and an irreversible reaction (the oxidation of water). Using this model it proved possible to obtain from any [Ce⁴⁺] *vs.* time decay trace a Tafel plot of the variation of current as a function of potential for the oxidation of water on the surface of the particles of RuO₂·*γ*H₂O*. In addition to providing valuable mechanistic information concerning this reaction, it also allowed the original kinetic traces to be reconstructed and decay curves simulated for a wide range of conditions. From the variation in Tafel plot data as a function of temperature, an activation energy for water oxidation of 52 ± 8 kJ mol⁻¹ was obtained.

1. Introduction

New materials capable of mediating efficiently the oxidation of water are of interest to many different groups, including those working in the areas of solar-to-chemical energy conversion¹ and electrocatalysis.² Over the years, during the search for such materials, an internationally recognised³⁻⁷ system for testing the catalytic activity of a promising catalyst material has been developed, in which Ce^{IV} ions, in 0.5 mol dm⁻³ H₂SO₄, are used to oxidise water to O₂, *i.e.*



This 'test' system has several limitations, including: (i) the pH of the solution must be < 1 to prevent extensive hydrolysis of the Ce^{IV} ions, and there are materials which only act as good O₂ catalysts at higher pH (*e.g.* Co²⁺ ions)⁸ and thus fail to be identified using the Ce^{IV} test system; (ii) the 'test' system does not really test the selectivity of the material as a redox catalyst for the oxidation of water rather than the oxidation of H₂, reduced relay (R⁻) or any other oxidisable moieties that are likely to be present in any practical system for the photodissociation of water; selectivity may be of importance if the catalyst is to be used in a water-splitting photochemical system. Despite these limitations, the Ce^{IV} test system has several important advantages over any other 'test' system (chemical or photochemical), including: (i) its simplicity and reproducibility; (ii) the long-term stability and ready availability of the oxidant; (iii) the general finding¹ that any material identified as a good O₂ catalyst using this test system appears also to be a

good O₂ catalyst when used at higher pH and/or with much less stable, expensive oxidants which can be generated photometrically, such as Ru(bpy)₃³⁺.

Using the Ce^{IV} test system, it has been found⁹⁻¹³ that most materials are either inert or subject to anodic corrosion under the highly oxidising conditions needed to oxidise water to O₂. Work carried out by our group^{9,10} and others^{11,12} has shown that highly hydrated ruthenium dioxide (RuO₂·xH₂O: H₂O content *ca.* 25%, *i.e.* $x = 2.46$) undergoes anodic corrosion when used as an O₂ catalyst. However, we have established¹³ recently that a mild heat treatment (*ca.* 144 °C for 5 h in air) of any sample of RuO₂·xH₂O (prepared or from a commercial source) transforms it into a stable, active O₂ catalyst of reaction (1). We refer to this new O₂ catalytic material as 'thermally activated ruthenium dioxide hydrate', or RuO₂·yH₂O* (typically, $y = 0.82$). When used as an O₂ redox catalyst in the Ce^{IV} test system stoichiometric amounts of O₂ are generated and the RuO₂·yH₂O* exhibits little or no evidence of corrosion, wear, poisoning or any other unwanted side-reactions which might lead to a loss in activity.¹³

In this paper we describe in detail the results of an extensive study of the kinetics of the oxidation of water by Ce^{IV} ions, mediated by RuO₂·yH₂O*. These results are interpreted using the theory developed in a previous paper,¹⁴ and based on an electrochemical model of redox catalysis, in which a highly reversible reaction (in this case: the reduction of the Ce^{IV} ions) is coupled to a highly irreversible reaction (in this case: the oxidation of water).

2. Experimental

2.1 Materials

The ruthenium dioxide hydrate was obtained from Johnson Matthey (batch no. 061151) and annealed at 140 °C in air for 5 h. All the Ce^{IV} sulphate solutions were prepared from an analytical volumetric solution of a 0.1 mol dm⁻³ Ce^{IV} sulphate solution using 0.5 mol dm⁻³ H₂SO₄ (AnalaR) as the diluent. The Ce^{III} sulphate solutions were prepared by reduction of the 0.1 mol dm⁻³ Ce^{IV} sulphate solution with a small excess of a non-stabilised 30% hydrogen-peroxide solution. Any residual hydrogen peroxide in the Ce^{III} solution was destroyed by refluxing the solution for 1 h, as revealed by testing with Ti(SO₄)₂ and with dichromate/ether. Subsequent dilutions were made with 0.5 mol dm⁻³ H₂SO₄ (AnalaR). Unless stated otherwise, all chemicals were purchased from BDH, and the water used was doubly distilled and deionised.

2.2 Preparation and Handling of a Stock Dispersion

It is essential for any kinetic study involving a heterogeneous dispersion to be able to reproduce that dispersion consistently. For this reason the following simple but effective method was devised for producing a consistent stock dispersion of RuO₂·yH₂O*. Initially, 20 mg of RuO₂·yH₂O* powder was dispersed in 100 cm³ of 0.5 mol dm⁻³ H₂SO₄ contained in a 250 cm³ Quickfit stoppered conical flask containing a 25 mm Teflon-coated magnetic stirrer bar. Dispersion of the catalyst powder was achieved by placing the flask in an ultrasound bath (Ultra Sonics, model 6442AE) for 10 min. The dispersion was then stirred for 48 h at a rate sufficient to maintain an even dispersion throughout the solution, with periodic shaking of the flask to resuspend any dioxide adhering to the flask walls, a tendency which diminished significantly over the 48 h. The final product was a dispersion which, even if allowed to settle, was readily resuspended by shaking and which provided results of acceptable consistency in our kinetic work. However, even with these precautions the mean activity of the dispersion was still seen to rise by *ca.* 10% in 10 days, possibly due to the mechanical grinding action of the stirrer bar. As a result, after this period of time the dispersion was discarded and a fresh stock dispersion prepared.

2.3 Kinetic Studies

Aliquots of stock dispersion were placed into a 1 cm quartz fluorescence cell to which was added the quantity of Ce^{III} sulphate solution required for that particular experiment. The volume of solution in the cell was then made up to 2.8 cm^3 using 0.5 mol dm^{-3} H_2SO_4 (AnalaR). Using this procedure the dispersion concentrations could be readily set to any value over the range $0.02\text{--}0.2 \text{ g dm}^{-3}$, depending upon the initial aliquot of stock dispersion added; although, unless stated otherwise, the catalyst dispersion concentration used was fixed at 0.08 g dm^{-3} . The cell and its contents were placed in the thermostated (usually $30.00 \pm 0.01 \text{ }^\circ\text{C}$) sample cell holder of a Perkin-Elmer Lambda 3 spectrophotometer, where the contents were stirred continuously at a constant $1000 \text{ rev. min}^{-1}$ with a magnetically driven glass flea. The absorbance of the stirred cell contents which provides a measure of the extent of dispersion of the $\text{RuO}_2 \cdot y\text{H}_2\text{O}^*$ powder and its concentration, settled down to a constant value after 15–20 min and kinetic runs were carried out after this period.

Appropriate volumes and concentrations of Ce^{IV} sulphate solution in 0.5 mol dm^{-3} H_2SO_4 were injected into the stirred suspension using a 100 mm^3 gas-tight Hamilton syringe. Blank runs carried in the absence of catalyst showed that in all cases mixing was complete within *ca.* 5 s, a very short period compared to the timescale of the kinetics under study. The concentration of Ce^{IV} ions at any time, t , after injection, *i.e.* $[\text{Ce}^{4+}]_t$, was monitored spectrophotometrically at 430 nm or, in some cases, 320 nm for which the molar absorptivities (ϵ) are 290 and $5580 \text{ mol dm}^{-3} \text{ cm}^{-1}$, respectively.¹³

Each absorbance–time decay curve, due to the reduction of the Ce^{IV} ions, was recorded using a microcomputer (BBC Masterclass) in the form of 1000 absorbance values, each of 10-bit resolution, sampled at regular time intervals and stored subsequently on floppy disc. Kinetic data collected in this way were easily analysed for first- and second-order kinetics. In addition, numerical differentiation of the original decay curves, to produce the corresponding derivative-time profiles, was also carried out on the microcomputer.

2.4 Surface Area

In order to obtain a reliable and reproducible surface area, B.E.T. measurements are usually carried out on samples dried overnight at $200 \text{ }^\circ\text{C}$, under vacuum. Samples not treated in this way tend to give low and often irreproducible surface area when measured using the B.E.T. technique.¹⁵ However, the combination of high temperatures and vacuum would cause substantial changes in the nature of our $\text{RuO}_2 \cdot y\text{H}_2\text{O}^*$ sample; as a result the $\text{RuO}_2 \cdot y\text{H}_2\text{O}^*$ sample was degassed under vacuum for 15 h at only $25 \text{ }^\circ\text{C}$. The surface area of the $\text{RuO}_2 \cdot y\text{H}_2\text{O}^*$ sample used was then determined by a single-point nitrogen B.E.T. measurement and found to be $87 \text{ m}^2 \text{ g}^{-1}$. Although this method of degassing provided a reproducible value for the surface area of the $\text{RuO}_2 \cdot y\text{H}_2\text{O}^*$ sample, the efficiency of the degassing procedure is not known and thus this surface area value may be a conservative estimate.

3. Results and Discussion

3.1 The Electrochemical Model

Work carried out by our group has established¹³ that $\text{RuO}_2 \cdot y\text{H}_2\text{O}^*$ is able to mediate the oxidation of water by Ce^{IV} ions and that the catalyst is chemically inert under the reaction conditions used. Assuming that the redox couples involved will act independently of each other at the redox catalyst it is possible to predict the kinetics of catalysis from a knowledge of the current–voltage curves of the $\text{Ce}^{\text{IV}}/\text{Ce}^{\text{III}}$ and $\text{O}_2/\text{H}_2\text{O}$ couples.^{16,17}

The oxidation of water on ruthenium dioxide, hydrated or anhydrous, has been the source of numerous electrochemical studies¹⁸ and invariably the current–voltage curve is that for a highly irreversible reaction and fits a simple Tafel-type equation,¹⁹ *i.e.*

$$i_{\text{O}_2} = i_w \exp(2.303\eta/b) \quad (2)$$

where, i_w is the exchange current for water oxidation, b is the Tafel slope and η is the overpotential. The overpotential represents the difference between the applied potential (E_{ap}) and the equilibrium potential for the O₂/H₂O couple (E_w° ; taken to be 1.23 V *vs.* NHE).

In contrast to the oxidation of water, electrochemical studies have not been carried out on the Ce^{IV}/Ce^{III} couple using ruthenium dioxide or its hydrates as the electrode material and, therefore, the current–voltage curve for this couple is unknown. However, it is very likely that the exchange current density is much greater than that for water. In the limit, if the heterogeneous rate constant for electron transfer (k_o) between Ce^{IV} and Ce^{III} ions on the surface of a RuO₂· γ H₂O* particle is much greater than the mass-transfer coefficient (k_d) for the Ce^{IV} and Ce^{III} ions to the particle, then the current–voltage curve for the Ce^{IV}/Ce^{III} couple will be that for a Nernstian reaction and given by the equation

$$E_{\text{ap}} = E_{\text{Ce}}^\circ + (RT/F) \ln [(i - i_{1,c}) / (i_{1,a} - i)] \quad (3)$$

where E_{Ce}° is the formal potential of the Ce^{IV}/Ce^{III} couple (taken to be 1.445 V *vs.* NHE at 30 °C) and $i_{1,a}$ and $i_{1,c}$ are the limiting anodic (positive) and cathodic (negative) current, respectively.¹⁹ Eqn (3) makes the assumption that the mass-transfer coefficients for Ce^{IV} and Ce^{III} ions have approximately the same value, k_d . The constant, k_d , depends inversely upon the diffusion layer thickness, δ , which in turn depends upon the hydrodynamic flow conditions around the electrode. In order to keep δ constant for the RuO₂· γ H₂O* powder particles, all dispersions were stirred at a fixed rate of 1000 rev. min⁻¹.

There is some tentative evidence that k_o may be $> k_d$ for the RuO₂· γ H₂O* microelectrode particles. For example, the exchange current density, and therefore k_o , for the Fe³⁺/Fe⁴⁺ couple on hydrous metal-oxide electrodes is similar to that for platinum.²⁰ However, the exchange-current density for the Ce^{IV}/Ce^{III} couple in 0.5 mol dm⁻³ H₂SO₄ has been determined²¹ for Pt and corresponds to a k_o value of 5×10^{-4} cm s⁻¹. We shall, for the moment, make the assumption that k_o for RuO₂· γ H₂O* is similar to that for Pt, *i.e.* 5×10^{-4} cm s⁻¹. In a study²² of the kinetics of the oxidation of brine to chlorine by Ce^{IV} ions, mediated by RuO₂· γ H₂O*, the rate of Ce^{IV} reduction was found to be diffusion-controlled and, from the data reported, a value of $k_d = 7.2 \times 10^{-5}$ cm s⁻¹ can be calculated. The combination of these estimates of k_o and k_d for RuO₂· γ H₂O* suggest that k_d may well be sufficiently $< k_o$ that the current–voltage curve for this couple on RuO₂· γ H₂O* will be described by eqn (3).

Following on from eqn (3), the cathodic current ($i_{c,t}$) per cm³ flowing through the redox catalyst at a potential, $E_{\text{mix},t}$, at any time, t , will be given by:

$$-i_{c,t} = \frac{k_d F A_{\text{cat}} \{ [Ce^{4+}]_t - [Ce^{3+}]_t \exp F(E_{\text{mix},t} - E_{\text{Ce}}^\circ) / RT \}}{\exp F(E_{\text{mix},t} - E_{\text{Ce}}^\circ) / RT} \quad (4)$$

where A_{cat} is the effective surface area of the redox catalyst dispersion per cm³ and $[Ce^{4+}]_t$ and $[Ce^{3+}]_t$ are the concentrations (in mol cm⁻³) of the Ce^{IV} and Ce^{III} ions at time, t . In accordance with the additivity principle, $-i_c = i_a = i_{\text{mix}}$, where i_a is the anodic current flowing through the catalyst dispersion due to the irreversible oxidation of water, and is given by eqn (2), in which $\eta = E_{\text{mix}} - E_w^\circ$.

For any decay trace the rate of reduction of the Ce^{IV} ions at any time, t , is $d(t)$ (mol s⁻¹ cm⁻³), where $d(t) = d[Ce^{4+}]_t/dt$. This rate is related directly to i_{mix} by the expression

$$d(t) = i_{\text{mix}}/F. \quad (5)$$

Since we are dealing with a heterogeneous system it is more appropriate to discuss the kinetics in terms of the rate of a chemical surface reaction [*i.e.* $R_{\text{mix}}(t)$], which has units of equiv. $\text{s}^{-1} \text{cm}^{-2}$. This heterogeneous rate is related to i_{mix} and $d(t)$ as follows:

$$R_{\text{mix}}(t) = i_{\text{mix}}/FA_{\text{cat}} = d(t)/A_{\text{cat}} \quad (6)$$

If, when studying the kinetics of reaction (1), both the initial concentrations of Ce^{IV} and Ce^{III} ions are known, as is usually the case, then, by monitoring the disappearance of the Ce^{IV} ions as a function of time, we can obtain both $[\text{Ce}^{4+}]_t$ and $[\text{Ce}^{3+}]_t$ at any time, t . From $d(t)$, the derivative of the $[\text{Ce}^{4+}]$ vs. time curve at time, t , we can also determine $i_{\text{mix},t}$ and $R_{\text{mix}}(t)$, via eqn (5) and (6). A knowledge of $R_{\text{mix}}(t)$ then allows us to calculate the mixture potential at time t (*i.e.* $E_{\text{mix},t}$) at the $\text{RuO}_2 \cdot y\text{H}_2\text{O}^*$ microelectrode particles using a modified and rearranged version of eqn (4), *i.e.*

$$E_{\text{mix},t} = E'_{\text{Ce}} + (RT/F) \ln \{ [-k_d[\text{Ce}^{4+}]_t - R_{\text{mix}}(t)] / [R_{\text{mix}}(t) - k_d[\text{Ce}^{3+}]_t] \} \quad (7)$$

provided k_d is known.

A major prediction of the kinetics for a Nernstian reduction reaction coupled to a highly irreversible oxidation reaction is that a plot of $E_{\text{mix},t}$ vs. $\log[R_{\text{mix}}(t)]$ should produce a straight line of gradient b [see eqn (2)] and intercept $-b \log(R_w)$, where

$$R_w = [i_w \exp(-2.303E_w^0/b)] / FA_{\text{cat}} \quad (8)$$

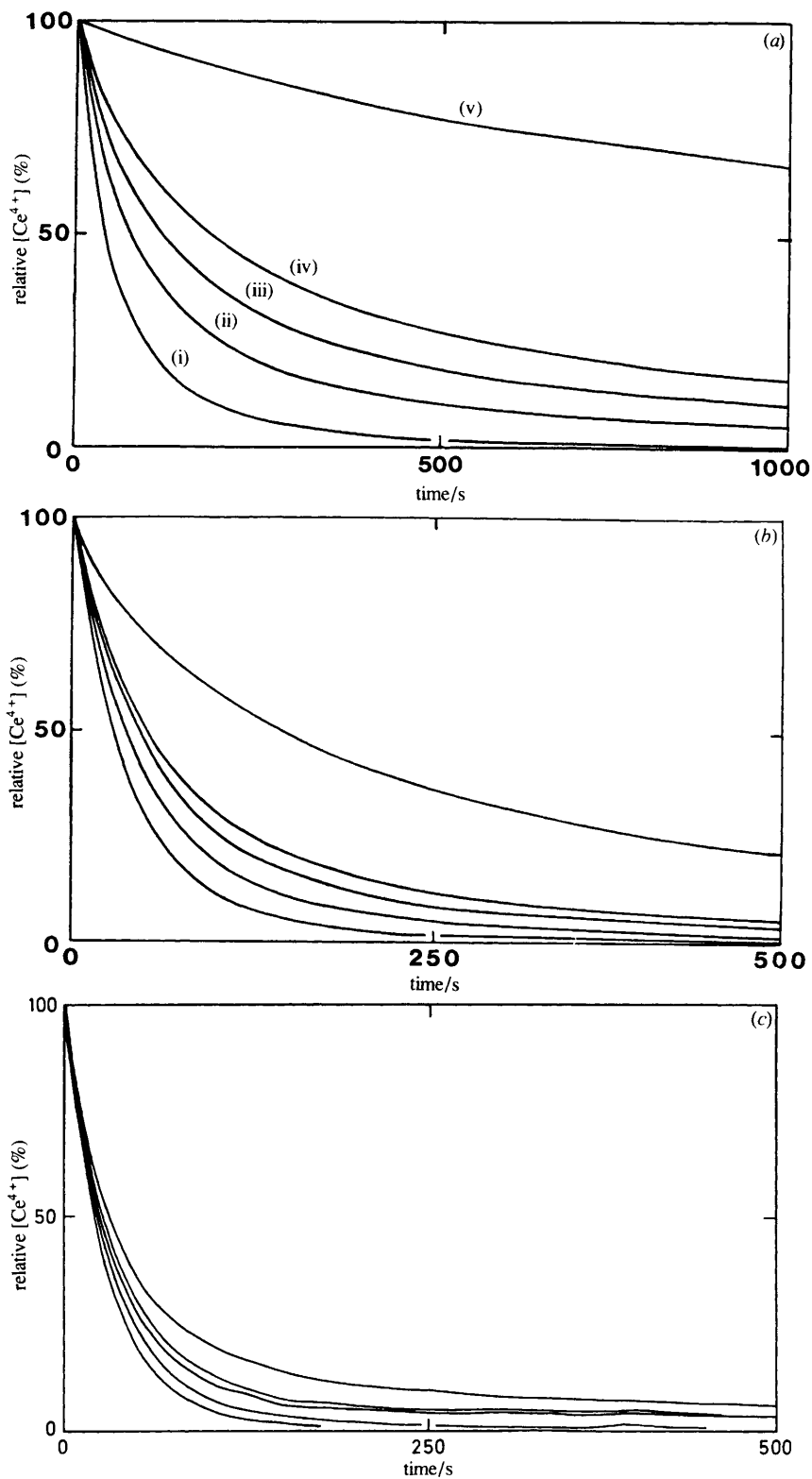
The applicability of our electrochemical model to catalysis of reaction (1) by $\text{RuO}_2 \cdot y\text{H}_2\text{O}^*$ particles can be tested via eqn (8), since both $R_{\text{mix}}(t)$ and $E_{\text{mix},t}$ can be determined for any of our kinetic runs using eqn (6) and (7), respectively.

3.2 Inhibition by Ce^{III} Ions

The inhibitory effect of Ce^{III} ions on the kinetics of reaction (4) was most clearly observed in a series of experiments in which 100 mm^3 of a $0.1 \text{ mol dm}^{-3} \text{ Ce}^{\text{IV}}$ sulphate solution was injected into 2.8 cm^3 of a $0.5 \text{ mol dm}^{-3} \text{ H}_2\text{SO}_4$ solution containing different concentrations of Ce^{III} ions, but always a fresh catalyst dispersion (0.086 g dm^{-3}); after mixing, the initial Ce^{IV} ion concentration ($[\text{Ce}^{4+}]_0$) was $3.45 \times 10^{-3} \text{ mol dm}^{-3}$. Fig. 1(a) illustrates the Ce^{IV} ion decay curves, (i), (ii), (iii), (iv) and (v), recorded directly after mixing, when the initial $\text{Ce}^{\text{IV}}/\text{Ce}^{\text{III}}$ concentration ratios (*i.e.* $[\text{Ce}^{4+}]_0/[\text{Ce}^{3+}]_0$) were 1:0, 1:1, 1:2, 1:3 and 1:10, respectively. Interestingly, the inhibitory effect of the presence of Ce^{III} ions on the rate of reaction (1) appeared to decrease as the $[\text{Ce}^{4+}]_0$ was decreased. This effect is illustrated by fig. 1(b) and 1(c) in which the $[\text{Ce}^{4+}]_0$ was 3.45×10^{-4} and $3.45 \times 10^{-5} \text{ mol dm}^{-3}$, respectively. In each of fig. 1(b) and 1(c), the five curves illustrated correspond, from left to right, to injections of Ce^{IV} ions which produced $[\text{Ce}^{4+}]_0/[\text{Ce}^{3+}]_0$ ratios of: 1:0 (fastest), 1:1, 1:2, 1:3 and 1:9 (slowest), respectively.

Decay curves identical to those illustrated in fig. 1 were also obtained by repeated injection of a Ce^{IV} solution which produced the same $[\text{Ce}^{4+}]_0$ as in fig. 1, *i.e.* 3.45×10^{-3} , 3.45×10^{-4} and $3.45 \times 10^{-5} \text{ mol dm}^{-3}$, respectively, into a single catalyst dispersion. In this set of experiments the $[\text{Ce}^{4+}]_0/[\text{Ce}^{3+}]_0$ ratio decreased as the number of injections of Ce^{IV} ions was increased. Since this method produced the same decay curves as those illustrated in fig. 1, it would appear that the redox catalyst does not lose activity even after repeated use. Further evidence of this was obtained by extracting the catalyst after extensive use and, after washing and redispersing, testing it for catalytic activity. No loss in activity of the catalyst treated in this manner was observed compared to that of a fresh sample. In addition to our group,²³ others²⁴ have also noted the inhibitory action of Ce^{III} ions on the kinetics of reaction (1).

The initial first-order rate constant for the reduction of Ce^{IV} ions via reaction (1), *i.e.* $k_i = d(t=0)/[\text{Ce}^{4+}]_0$ (units: s^{-1}), was studied as a function of $[\text{Ce}^{4+}]_0$ over the range 3.45×10^{-3} – $3.45 \times 10^{-5} \text{ mol dm}^{-3}$, with $[\text{Ce}^{3+}]_0$ ca. 0 mol dm^{-3} . Advantage was taken of

Oxidation of Water by Ce^{IV} Ions

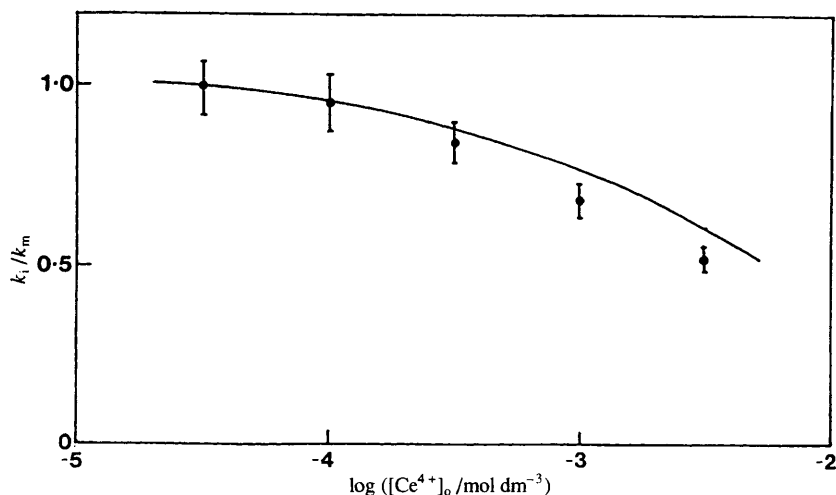


Fig. 2. Plot of k_i/k_m vs. $\log([Ce^{4+}]_o/mol\ dm^{-3})$; k_m is the experimentally determined value of k_i when $[Ce^{4+}]_o = 3.45 \times 10^{-5}\ mol\ dm^{-3}$ and was determined as $0.032\ s^{-1}$. The solid line was calculated using eqn (4).

the approximately first-order nature of the Ce^{IV} ion decay over its first half-life to provide a measure of k_i and its observed variation with $[Ce^{4+}]_o$ is illustrated in fig. 2. From fig. 2 it appears that, at very low values of $[Ce^{4+}]_o$, k_i tends to a limiting value, which we have called k_m , where $k_m = 0.032\ s^{-1}$. This trend in k_i is predicted by the electrochemical model *via* eqn (4), since, with $[Ce^{3+}]_o \approx 0$, a decrease in $[Ce^{4+}]_o$ will lower E_{mix} and, thus, increase i_{mix} . In the limit, as $[Ce^{4+}]_o$ tends to $0\ mol\ dm^{-3}$, i_{mix} will tend to its limiting value, $-i_{1,c}$. The results illustrated in fig. 2 indicate that at $[Ce^{4+}]_o = 3.45 \times 10^{-5}\ mol\ dm^{-3}$, the rate of Ce^{IV} reduction is very close to being wholly diffusion-controlled and, as a result, k_m is a good approximation of the first-order diffusion-controlled rate constant for the reduction of Ce^{IV} ions on $RuO_2 \cdot yH_2O^*$ particles. Knowledge of this homogeneous first-order constant allows us to calculate its heterogeneous counterpart, k_d , using this equation

$$k_d = k_m/A_{cat} \quad (9)$$

From this work k_d was estimated as *ca.* $4.6 \times 10^{-4}\ cm\ s^{-1}$.

3.3 Diffusion-controlled Nernstian-current Kinetics

The findings reported above suggest that at an initial $[Ce^{4+}] = 3.45 \times 10^{-5}\ mol\ dm^{-3}$ and $[Ce^{3+}]$ *ca.* $0\ mol\ dm^{-3}$, the rate of reduction of Ce^{IV} ions *via* reaction (1) is diffusion-controlled. Under such conditions the mixture current at any time, t , will be given by:

$$i_{mix,t} \approx -i_{1,c} = Fk_d A_{cat}[Ce^{4+}]_t \quad (10)$$

A number of experiments were carried out in which $100\ mm^3$ of a solution containing $0.001\ mol\ dm^{-3}$ Ce^{IV} ions in $0.5\ mol\ dm^{-3}$ H_2SO_4 were injected into $2.8\ cm^3$ of a

Fig. 1. Relative concentration (of Ce^{IV} ions) vs. time curves when $[Ce^{4+}]_o$ was: (a) 3.45×10^{-3} , (b) 3.45×10^{-4} , or (c) $3.45 \times 10^{-5}\ mol\ dm^{-3}$, respectively. In each of the figures the five decay curves were recorded under conditions of different $[Ce^{3+}]_o$. Thus, for (a), the $[Ce^{4+}]_o/[Ce^{3+}]_o$ were: (i) 1:0 (fastest), (ii) 1:1, (iii) 1:2, (iv) 1:4 and (v) 1:10 (slowest). For (b) and (c), the $[Ce^{4+}]_o/[Ce^{3+}]_o$ ratios were: 1:0 (fastest), 1:1, 1:2, 1:3 and 1:9 (slowest). All other conditions were as described in section 2.3.

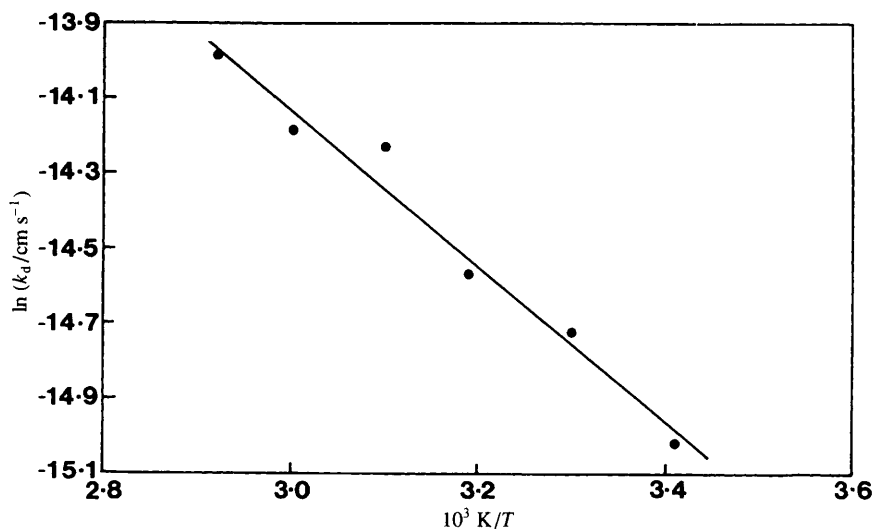


Fig. 3. Plot of $\ln(k_d/\text{cm s}^{-1})$ vs. $10^3 K/T$. In this experiment the $[\text{Ce}^{4+}]_0$ was very low ($3.45 \times 10^{-5} \text{ mol dm}^{-3}$) and the $[\text{Ce}^{3+}]_0$ ca. 0 mol dm^{-3} .

dispersion of $\text{RuO}_2 \cdot y\text{H}_2\text{O}^*$ to produce an initial Ce^{IV} concentration of $3.45 \times 10^{-5} \text{ mol dm}^{-3}$. In one set of these experiments the observed initial homogeneous first-order diffusion-controlled rate constant (k_m) was measured as a function of catalyst concentration over the range $0.02\text{--}0.2 \text{ g dm}^{-3}$. A plot of $\log(k_m/\text{s}^{-1})$ vs. $\log\{[\text{redox catalyst}]/(\text{g dm}^{-3})\}$ produced a good straight line [number of points (n) = 6; correlation coefficient (r) = 0.9981] of gradient (m) = 1.14 ± 0.08 and intercept (c) = 0.56 ± 0.2 . From the value for the gradient the rate of reaction (1) appears to depend directly upon the redox catalyst concentration, which is in agreement with the electrochemical model [see eqn (10)], since the surface area available for catalysis per cm^3 of solution, *i.e.* A_{cat} , will be related directly to [redox catalyst]. A mean value of $(4.4 \pm 0.1) \times 10^{-4} \text{ cm s}^{-1}$ for k_d was calculated *via* eqn (9) from the results of the above work and the measured surface area of $\text{RuO}_2 \cdot y\text{H}_2\text{O}^*$ (see section 2.4). This value for k_d is only slightly lower than the estimated value for k_0 (see section 3.1), indicating that k_d may not be $\gg k_0$ and that the kinetics for the reduction of Ce^{IV} ions in reaction (4) may not be fully Nernstian as we have assumed (see section 3.1). If, however, as we shall show, the reduction of the Ce^{IV} ions appears to be a Nernstian reaction, then this casts doubt on the assumption made previously that k_0 for $\text{RuO}_2 \cdot y\text{H}_2\text{O}^*$ is the same as that for Pt, and/or that the value of the surface area used to calculate k_d was the true value and not an underestimate (see section 2.4).

In another set of experiments, in which $[\text{Ce}^{4+}]_0 = 3.45 \times 10^{-6} \text{ mol dm}^{-3}$, the heterogeneous first-order rate constant for the reduction of the Ce^{IV} ions, where the $[\text{Ce}^{4+}]_0 = 3.45 \times 10^{-5} \text{ mol dm}^{-3}$, was determined as a function of temperature over the range $20\text{--}70 \text{ }^\circ\text{C}$ and fig. 3 illustrates the Arrhenius plot of the results. From the gradient of this plot an activation energy of $17.2 \pm 0.1 \text{ kJ mol}^{-1}$ was derived, which compares very favourably with that expected for a diffusion-controlled reaction,²⁵ *i.e.* typically ca. 15 kJ mol^{-1} .

3.4 Partly Diffusion-controlled Nernstian-current Kinetics

From fig. 2 it is apparent that, as the initial concentration of Ce^{IV} ions is increased from 3.45×10^{-5} to $3.45 \times 10^{-3} \text{ mol dm}^{-3}$, the initial homogeneous first-order rate constant, k_1 ,

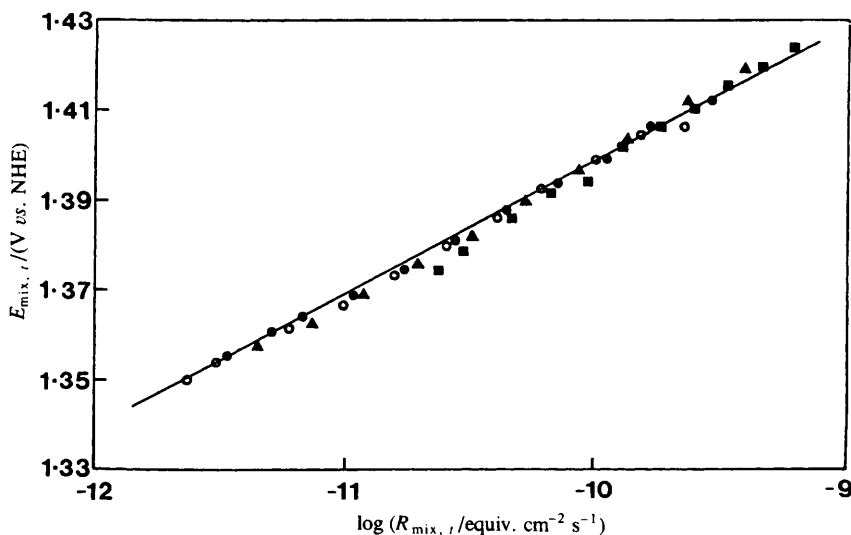
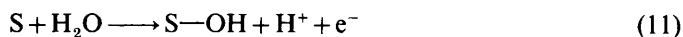


Fig. 4. Tafel plot of $E_{\text{mix},t}/(\text{V vs. NHE})$ vs. $\log(R_{\text{mix},t}/\text{equiv. cm}^{-2} \text{ s}^{-1})$. The data used to construct this plot are from fig. 1 (a), curves: (i) ■, (ii) ▲, (iii) ●, and, (iv) ○.

falls below k_m . Such changes are predicted by the electrochemical model and can be attributed to a shift in E_{mix} to more positive potentials which in turn causes a reduction in i_{mix} such that i_{mix} becomes $\ll -i_{1,c}$. Provided E_{mix} is not very close to the equilibrium potential for the $\text{Ce}^{\text{IV}}/\text{Ce}^{\text{III}}$ couple but sufficiently high that $-0.9i_{1,c} > i_{\text{mix}} > -0.1i_{1,c}$, then the kinetics will be partly diffusion-controlled and described by the combination of eqn (2) and (4).

For each of the decay curves illustrated in fig. 1 (a) we were able to calculate at any time, t , over three half-lives, both $R_{\text{mix}}(t)$, using eqn (6) and the derivative, $d(t)$, and $E_{\text{mix},t}$, using eqn (7) and $k_d = 4.4 \times 10^{-4} \text{ cm s}^{-1}$ (see section 3.3). As predicted by the electrochemical model, for each decay curve a plot of $E_{\text{mix},t}$ vs. $\log[R_{\text{mix}}(t)]$ produced a straight line with a common gradient and intercept; these plots are illustrated in fig. 4. A least-squares analysis of the data illustrated in fig. 4 produced the following information: $n = 80$, $r = 0.9968$, $m = 0.0309 \pm 0.0005 \text{ V per decade}$, $c = 1.708 \pm 0.006 \text{ V}$. From the values for the intercept and gradient the exchange current density, i_w/A_{cat} , units: A cm^{-2}) for the oxidation of water on the surface of the $\text{RuO}_2 \cdot \gamma\text{H}_2\text{O}^*$ powder particles can be calculated as *ca.* $(3.45 \pm 0.03) \times 10^{-11} \text{ A cm}^{-2}$, using eqn (8). At mixture potentials $< 1.36 \text{ V}$ there was evidence to suggest that the Tafel slope (b), and therefore possibly the mechanism, for water oxidation had changed. As a result, the current-exchange density calculated above was only a formal quantity and the true value may well be considerably smaller.

The oxidation of water to oxygen at the electrode surface may occur *via* the 'oxide pathway', *i.e.*



where S is the surface active site.²⁶ It can be shown that if reaction (11), (12), or (13) is the rate-determining step then the Tafel slope will be 120, 30, or 15 mV, respectively. Thus, we can interpret our observed Tafel slope of 30.9 mV per decade in terms of the 'oxide pathway', where reaction (12) is the rate-determining step. Interestingly, a

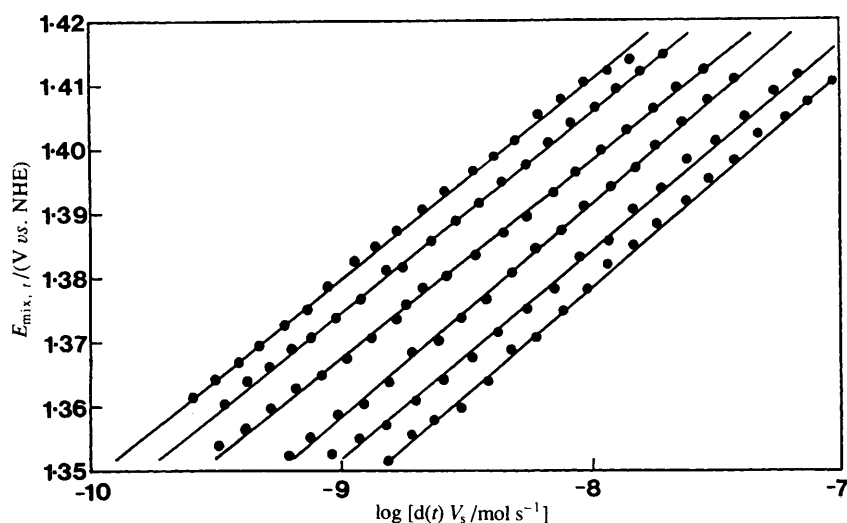


Fig. 5. Tafel plot of $E_{\text{mix},t}/\text{V vs. NHE}$ vs. $\log [d(t) V_s / \text{mol s}^{-1}]$ for a series of different catalyst concentrations. From left to right the plots correspond to a [redox catalyst] of: 21.8, 32.7, 49.0, 73.6, 110.3 and 165.5 mg dm^{-3} , respectively. In this work the $[\text{Ce}^{4+}]_0 = 3.45 \times 10^{-3} \text{ mol dm}^{-3}$ and the $[\text{Ce}^{4+}]_0 / [\text{Ce}^{3+}]_0$ ratio was 1:1.

number of electrochemical studies of the oxidation of water to O_2 have been carried out using high-defect hydrous ruthenium dioxide anodes,²⁷ a material which is likely to have similar electrochemical characteristics to $\text{RuO}_2 \cdot y\text{H}_2\text{O}^*$. In most cases the Tafel slope was also found to be 30 mV per decade and, coupled with other findings, was invariably interpreted, as we have done, in terms of the oxide pathway, with reaction (12) as the rate-determining step.^{20,28}

Using a $[\text{Ce}^{4+}]_0 / [\text{Ce}^{3+}]_0$ ratio of 1:1 and a $[\text{Ce}^{4+}]_0 = 3.45 \times 10^{-3} \text{ mol dm}^{-3}$, a series of decay curves was recorded for a variety of catalyst concentrations over the range 0.02–0.2 g dm^{-3} . A plot of $E_{\text{mix},t}$ vs. $\log [d(t) V_s]$, where V_s was the volume of solution in the reaction cell, was made for each of the decay curves and the resulting collection of straight lines is illustrated in fig. 5. Using the data in fig. 5 a plot of $\log [d(t) V_s]$ vs. $\log [\text{redox catalyst}]$ was made for three different set potentials, viz. 1.40, 1.38 and 1.36 V, vs. NHE resulting in three, almost parallel, straight lines with a mean value for the gradient of $ca. 1.25 \pm 0.05$. This finding is in support of the electrochemical model which predicts that $d(t)$ will depend directly upon A_{cat} , the effective surface area of the catalyst dispersion per cm^3 of solution, and therefore, directly upon [redox catalyst] [see eqn (5)].

In order to establish the activation energy of the water oxidation reaction, a set of experiments was conducted over a range of temperatures, 20–70 °C, with $[\text{Ce}^{4+}]_0 = 3.45 \times 10^{-3} \text{ mol dm}^{-3}$ and a $[\text{Ce}^{4+}]_0 / [\text{Ce}^{3+}]_0$ ratio of 1:4. A low $[\text{Ce}^{4+}]_0 / [\text{Ce}^{3+}]_0$ ratio was used since, in the absence of Ce^{III} ions, at the higher temperatures used in this set of experiments the reaction proceeded at a rate close to the diffusion-controlled rate, thus making eqn (7) ill-conditioned. In contrast, in the presence of a high initial concentration of Ce^{III} ions, the kinetics were considerably slower and, therefore, easily measured even up to 60 °C. Fig. 6 shows some of the typical decay curves recorded at different temperatures. In addition to studying the decay curves, the formal potential of the $\text{Ce}^{\text{IV}}/\text{Ce}^{\text{III}}$ couple was determined as a function of temperature, and the results are illustrated in fig. 7. At each temperature, the observed decay curve, see fig. 6, was analysed over three half-lives and used to generate a set of $E_{\text{mix},t}$ vs. $\log [R_{\text{mix}}(t)]$ data; the value used for E_{Ce}° in eqn (4) was taken from the curve in fig. 7. The Tafel plots

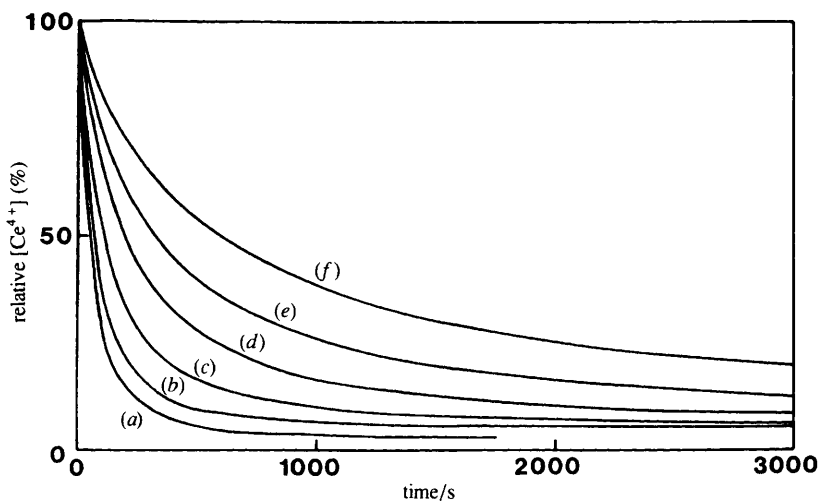


Fig. 6. Relative concentration (of Ce^{IV} ions) vs. time, recorded at different temperatures, with $[\text{Ce}^{\text{IV}}]_0 = 3.45 \times 10^{-3} \text{ mol dm}^{-3}$ and $[\text{Ce}^{\text{IV}}]_0/[\text{Ce}^{\text{III}}]_0 = 1:4$. The plots correspond to runs made at: (a) 20, (b) 30, (c) 40, (d) 50, (e) 60 and (f) 70 °C.

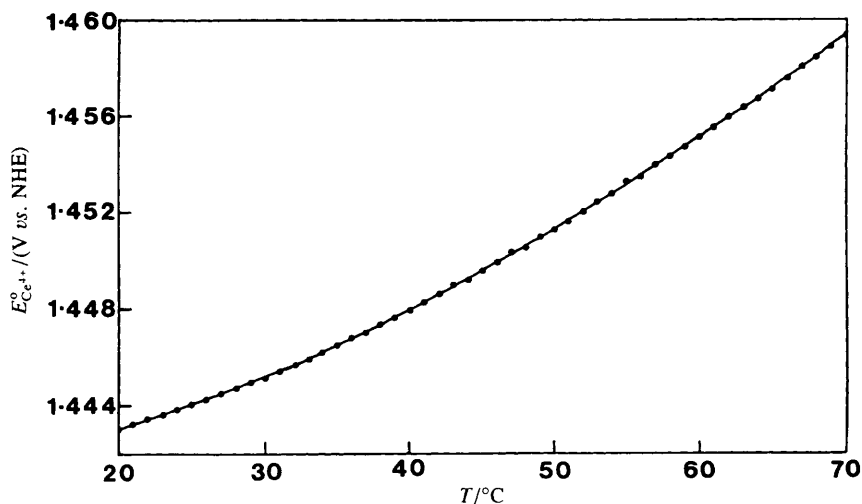


Fig. 7. Observed variation of the formal potential ($[\text{Ce}^{\text{IV}}]_0/[\text{Ce}^{\text{III}}]_0 = 1:1$) of the $\text{Ce}^{\text{IV}}/\text{Ce}^{\text{III}}$ redox couple in $0.5 \text{ mol dm}^{-3} \text{ H}_2\text{SO}_4$ as a function of temperature.

calculated from the decay curves illustrated in fig. 6 are themselves plotted in fig. 8. From the results illustrated in fig. 8 it appears that at mixture potentials $> 1.36 \text{ V vs. NHE}$ all the Tafel plots are straight lines with an approximately common slope (ca. 30.1 mV per decade). However, at $E_{\text{mix},t} < 1.36 \text{ V vs. NHE}$ a deviation to a lower Tafel slope value is apparent, indicating possibly a change of mechanism at these low overpotentials. This can be rationalised in terms of the oxide pathway mechanism, since as the potential on the $\text{RuO}_2 \cdot y\text{H}_2\text{O}^*$ particles falls so will the surface coverage of S-O species. Eventually, a point may be reached when reaction (13) becomes rate-limiting and, as a result, the Tafel slope will be expected to change to 15 mV per decade.^{26, 27}

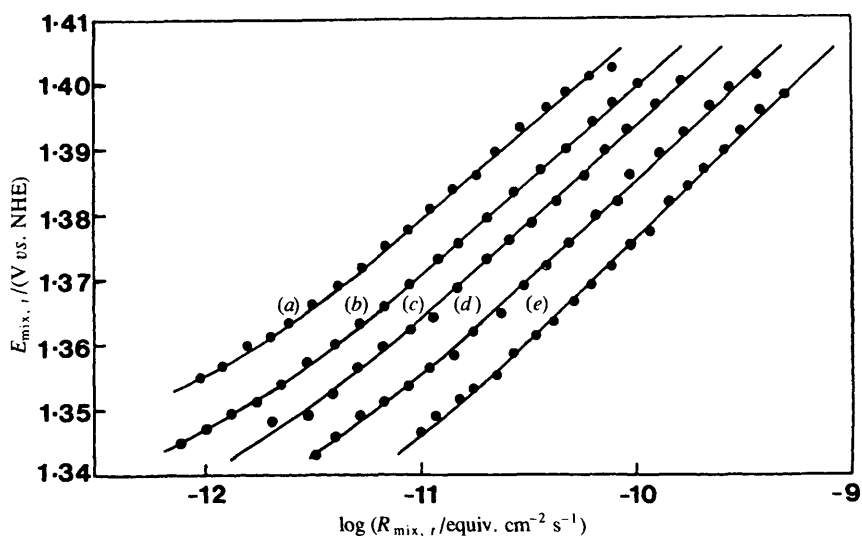


Fig. 8. Tafel plot of $E_{\text{mix},t}/(\text{V vs. NHE})$ vs. $\log[R_{\text{mix},t}/(\text{equiv. cm}^{-2} \text{s}^{-1})]$, calculated using the data illustrated in fig. 6 and 7. The plots correspond to runs made at: (a) 20, (b) 30, (c) 40, (d) 50, and (e) 60 °C.

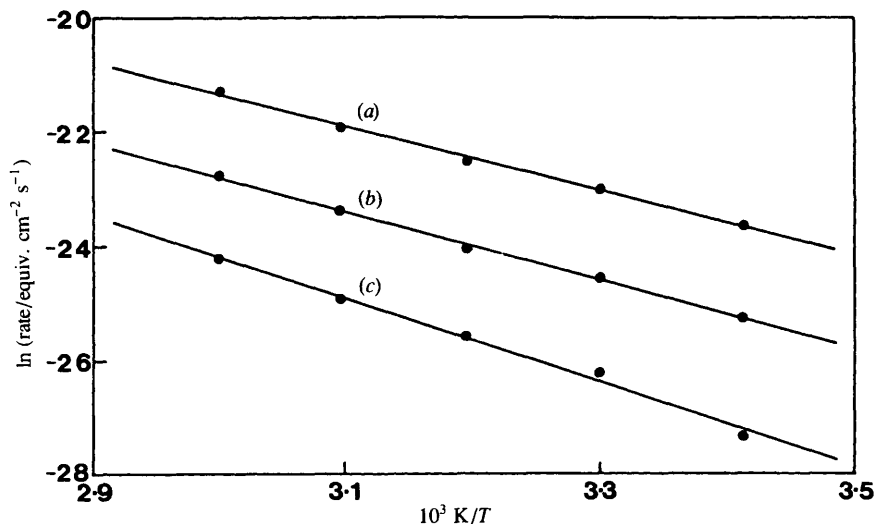


Fig. 9. Arrhenius plots of the variation with temperature of the heterogeneous rate constant (R_{mix}) at different calculated values of catalyst potential (E_{mix}); data taken from fig. 8. The plots correspond to E_{mix} values of (a) 1.40, (b) 1.38 and (c) 1.36 V vs. NHE.

Arrhenius plots, shown in fig. 9, were constructed by taking the rate value from each Tafel plot at a series of fixed potentials, 1.40, 1.38 and 1.36 V vs. NHE. From the gradients of the three, approximately parallel, straight lines, see fig. 9, a mean activation energy for the oxidation of water to O_2 on the surface of the $\text{RuO}_2 \cdot \gamma\text{H}_2\text{O}^*$ particles was calculated to be $52 \pm 8 \text{ kJ mol}^{-1}$. This value for the activation energy compares favourably with the value of 50.4 kJ mol^{-1} , determined previously by another group,²⁸

in a macroelectrode study of the oxidation of water using a hydrous ruthenium dioxide anode.

3.5 Simulation of the Kinetic Curves

The pertinence of the electrochemical model used here, its assumptions, mathematical description and the accuracy of our analysis based upon the model are best assessed by the solution and integration of eqn (2) and (4) in conjunction with our estimated values for the constants involved; these constants include: $R_w = 2.69 \times 10^{-16}$ equiv. $\text{cm}^{-2} \text{s}^{-1}$, $b = 30$ mV per decade and $k_d = 4 \times 10^{-4}$ cm s^{-1} . Using Newton's method and the combination of eqn (2) and (4), it can be shown that for any known values of $[\text{Ce}^{4+}]_o$ and $[\text{Ce}^{3+}]_o$, the mixture potential on the particle can be determined, E_{mix} , which, in turn, can be used to calculate i_{mix} , using eqn (2).¹ Provided the initial concentrations of Ce^{IV} and Ce^{III} ions are known, this routine coupled to a variable step version of Euler's method may be combined to regenerate any of the observed $[\text{Ce}^{4+}]$ vs. time decay curves and used to predict the shapes of decay traces under very different reaction conditions. A detailed description of the procedure has been described in a previous paper.¹⁴

Fig. 10(a)–(c) illustrates reconstructed versions of the decay curves given in fig. 1(a)–(c), respectively. The fit to the experimentally determined decay curves at $[\text{Ce}^{4+}]_o = 3.45 \times 10^{-4}$ and 3.45×10^{-3} mol dm^{-3} is very good but at $[\text{Ce}^{4+}]_o = 3.45 \times 10^{-5}$ mol dm^{-3} the experimental curves are marginally, but consistently, faster than the simulated curves. This may be because our estimate of k_d is slightly low, by *ca.* 9%, although such an underestimate would only give rise to significant error when $[\text{Ce}^{3+}]_o = 0$ mol dm^{-3} . However, it must be recognised that the model does not take into account the non-steady-state process of catalyst charging, which occurs when the Ce^{IV} ions and the catalyst are first mixed. The inner-layer capacitance (C_i) of ruthenium dioxide, produced by heating RuCl_3 at 400 °C for 5 h has been reported¹⁶ as 6.4×10^{-5} F cm^{-2} . In 0.5 mol dm^{-3} H_2SO_4 , both the ionic strength and RuO_2 surface potential are high; thus the diffuse-layer capacitance will be large and exert little influence on the overall capacitance (C), so that $C = C_i$. Assuming that C_i for $\text{RuO}_2 \cdot y\text{H}_2\text{O}^*$ is similar to that for RuO_2 , then in the experiments in which $[\text{Ce}^{4+}]_o = 3.45 \times 10^{-5}$ mol dm^{-3} and $[\text{redox catalyst}] = 0.086$ g dm^{-3} , the concentration of Ce^{IV} ions used to charge up the catalyst to 1.36 V (the approximate initial value of E_{mix} in these experiments) = *ca.* 6×10^{-6} mol dm^{-3} , which represents 19% of the initial Ce^{IV} ion concentration. The charging process would be expected to be diffusion-controlled and therefore may appear slightly faster than even the steady-state diffusion-controlled kinetics predicted by the electrochemical model, since in the latter the steady-state diffusion layer would not have been fully formed. At higher Ce^{IV} concentrations the charging-up step will have a much less significant effect on the observed $[\text{Ce}^{4+}]$ vs. time profile; thus the fit between simulated and observed decay curves should be better, as was found.

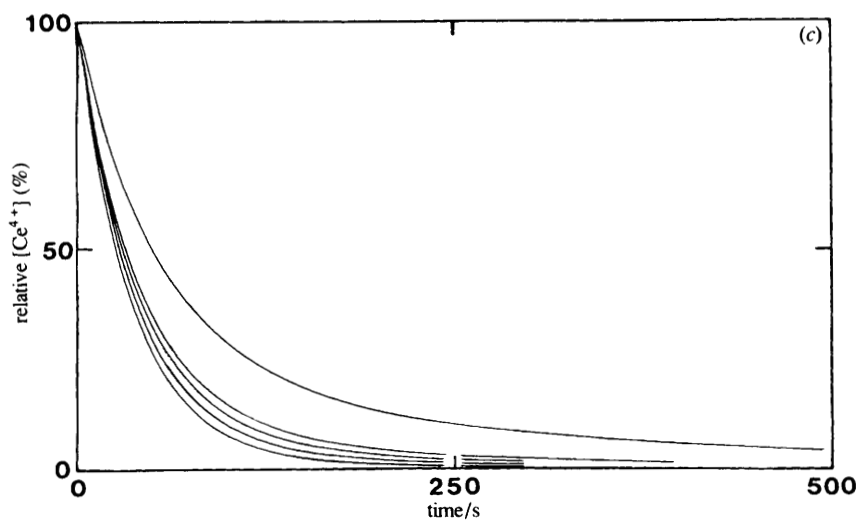
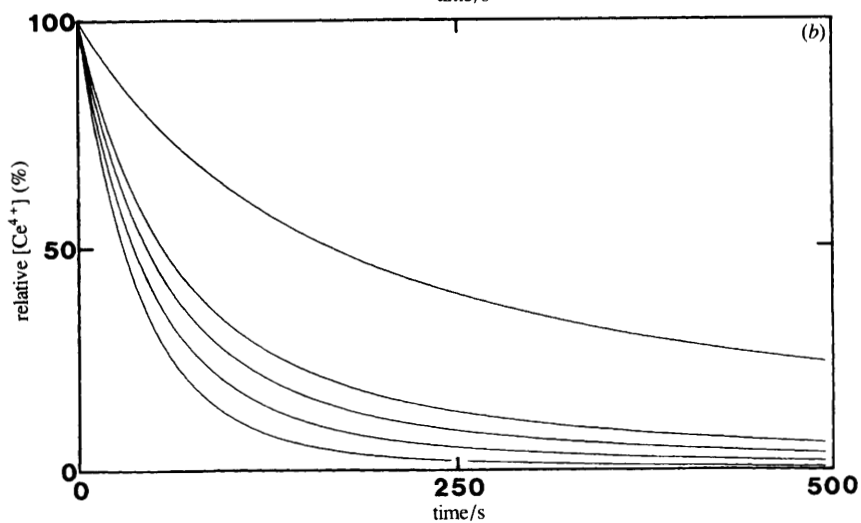
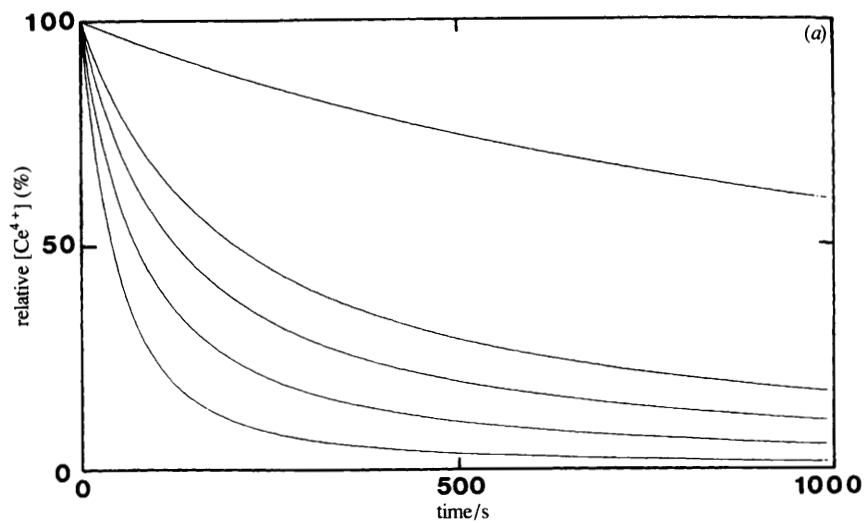
3.6 Activation-controlled Nernstian-current Kinetics

At high Ce^{IV} ion concentrations and a low $[\text{Ce}^{4+}]/[\text{Ce}^{3+}]$ ratio, the current will be significantly less than the diffusion-limited rate and the $[\text{Ce}^{3+}]$ will be approximately constant and equal to $[\text{Ce}^{3+}]_o$, as the reaction proceeds. Under these conditions the electrochemical model predicts that the kinetics may become activation-controlled and described by the equation:

$$R_{\text{mix}}(t) = R_w \exp(2.303E_{\text{Ce}}^o/b) \times k_d[\text{Ce}^{3+}]_o^{-\beta} \times k_d[\text{Ce}^{4+}]^\beta \quad (14)$$

where

$$\beta = 2.303RT/Fb. \quad (15)$$

Oxidation of Water by Ce^{IV} Ions

Since, at mixture potentials > 1.36 V *vs.* NHE, b is *ca.* 0.030 mV, then, substituting into eqn (15) reveals $\beta = 2$, which indicates that under these conditions the reaction kinetics should be second-order with respect to $[\text{Ce}^{4+}]$. In the experiments used for the determination of the activation energy of the oxidation of water, see fig. 7–9, a high $[\text{Ce}^{4+}]_0$ (3.45×10^{-3} mol dm $^{-3}$) and a low $[\text{Ce}^{4+}]/[\text{Ce}^{3+}]$ ratio (1:4) was used and, as predicted, at mixture potentials > 1.36 V *vs.* NHE, where i_{mix} was typically $\ll -0.14 \times i_{1,e}$, the $[\text{Ce}^{4+}]$ decay curves gave good straight lines for a second-order plot of the type $[\text{Ce}^{4+}]_t^{-1}$ *vs.* time.

4. Conclusion

The observed kinetics for the oxidation of water by Ce^{IV} ions, mediated by a dispersion of $\text{RuO}_2 \cdot y\text{H}_2\text{O}^*$ powder particles, can be readily interpreted using an electrochemical model of redox catalysis in which it is assumed that the catalyst particles act as microelectrodes; providing a medium in which electron transfer can take place between a highly irreversible oxidation reaction (the oxidation of water) and a Nernstian reduction reaction (the reduction of Ce^{IV} ions).

We thank Dr Peter Douglas for many useful discussions, the University of Wales for a postgraduate studentship for N.M. and the S.E.R.C. for supporting this work.

References

- 1 *Energy Resources through Photochemistry and Catalysis*, ed. M. Grätzel (Academic Press, New York, 1983).
- 2 S. Trasatti, *Electrochim. Acta*, 1984, **29**, 1503.
- 3 A. Mills, *J. Chem. Soc., Dalton Trans.*, 1982, 1213.
- 4 J. Kiwi and M. Grätzel, *Chemia*, 1979, **33**, 289.
- 5 G. Blondeel, A. Harriman, G. Porter, D. Urwin and J. Kiwi, *J. Phys. Chem.*, 1983, **87**, 2629.
- 6 R. Ramasamy, A. Kira and M. Kaneko, *J. Chem. Soc., Faraday Trans. 1*, 1987, **83**, 1539.
- 7 S. W. Gersten, G. J. Samuels and T. J. Meyer, *J. Am. Chem. Soc.*, 1982, **104**, 4029.
- 8 V. Ya. Shafirovich, M. K. Khannanov and V. V. Strelets, *Nouv. J. Chim.*, 1980, **4**, 81.
- 9 A. Mills, S. Giddings and I. Patel, *J. Chem. Soc., Faraday Trans. 1*, 1987, **83**, 2317.
- 10 A. Mills and M. L. Zeeman, *J. Chem. Soc., Chem. Commun.*, 1981, 948.
- 11 J. Kiwi, M. Grätzel and G. Blondeel, *J. Chem. Soc., Dalton Trans.*, 1983, 2215.
- 12 V. Ya. Shafirovich and V. V. Strelets, *Nouv. J. Chim.*, 1982, **6**, 183.
- 13 A. Mills, S. Giddings, I. Patel and C. Lawrence, *J. Chem. Soc., Faraday Trans. 1*, 1987, **83**, 2331.
- 14 A. Mills and N. McMurray, *J. Chem. Soc., Faraday Trans. 1*, 1989, **85**, 2047.
- 15 P. Siviglia, A. Daggetti and S. Trasatti, *Colloids Surf.*, 1983, **7**, 15.
- 16 M. Spiro and A. B. Ravnö, *J. Chem. Soc.*, 1965, 78.
- 17 M. Spiro, *Chem. Soc. Rev.*, 1986, **15**, 141.
- 18 S. Trasatti and G. Lodi, in *Electrodes of Conductive Metallic Oxides*, ed. S. Trasatti (Elsevier, Amsterdam, 1980), part B, p. 521, and references therein.
- 19 A. J. Bard and L. R. Faulkner, *Electrochemical Methods* (Wiley, New York, 1980), chap. 1 and 3.
- 20 S. Trasatti and G. Lodi, in *Electrodes of Conductive Metallic Oxides*, ed. S. Trasatti (Elsevier, Amsterdam, 1980), part A, p. 348.
- 21 M. Spiro, *Electrochim. Acta*, 1964, **9**, 1541.
- 22 A. Mills and A. Cook, *J. Chem. Soc., Faraday Trans. 1*, 1988, **84**, 1691.
- 23 A. Mills, C. Lawrence and R. Enos, *J. Chem. Soc., Chem. Commun.*, 1984, 1436.
- 24 J. Kiwi, *Isr. J. Chem.*, 1979, **18**, 369.
- 25 F. Wilkinson, *Chemical Kinetics and Reaction Mechanism* (Van Nostrand Reinhold, London, 1981), p. 140.

Fig. 10. Digitally simulated curves for initial Ce^{IV} ion concentrations of (a) 3.45×10^{-3} , (b) 3.45×10^{-4} and (c) 3.45×10^{-5} mol dm $^{-3}$. The five decay curves in each of the figures correspond to different $[\text{Ce}^{4+}]_0/[\text{Ce}^{3+}]_0$ ratios. These ratios are the same as those used to generate experimentally the curves illustrated in fig. 1(a)–(c).

- 26 J. O'M. Bockris, *J. Chem. Phys.*, 1956, **24**, 817.
- 27 S. Trasatti and W. E. O'Grady, in *Advances in Electrochemistry and Electrochemical Engineering*, ed. H. Gerischer and C. W. Tobias (Wiley, New York, 1981), **12**, p. 180 and references therein.
- 28 G. Lodi, E. Sivieri, A. de Battasti and S. Trasatti, *J. Appl. Electrochem.*, 1978, **8**, 135.

Paper 8/02864H; Received 15th July, 1988